Nonlinear Dyn
https://doi.org/10.1007/s11071-024-10534-w

RESEARCH

Numerical analyses of acoustic vibrational resonance in a Helmholtz resonator

K. A. Omoteso · O. Ozioko · O. Bagdasar · T. O. Roy-Layinde · U. H. Diala

Received: 24 June 2024 / Accepted: 18 October 2024

Abstract In this study, the numerical analyses of a system, which describes the motion of air particles in the cavity of a Helmholtz resonator (HR), excited by a sound wave, was conducted. The low-frequency (LF) signal in the acoustic field is amplitude-modulated by an additive high-frequency (HF) perturbation, which can enhance the detection of the low-frequency, through Vibrational Resonance (VR) phenomena. The focus was on the combined effect, of amplitude and frequency of the acoustic excitation, on the motion of particles and induction of resonance. It was demonstrated that the system exhibits several nonlinear behaviours, VR ceasing to exist for a particular motion of the particles, which is dictated by the excitation frequency in relation to the resonator's geometry. Furthermore, the regimes in which the performance of the system can be optimized, was identified, which facilitated the design of broadband acoustic resonators, suitable for most applications.

Keywords Nonlinear system · Helmholtz resonator · Acoustic waves · Vibrational resonance · Frequency domain

K. A. Omoteso · O. Ozioko · U. H. Diala (✉)
School of Engineering, University of Derby, Markeaton Street, Derby, UK
e-mail: U.diala@derby.ac.uk

K. A. Omoteso
e-mail: k.omoteso2@derby.ac.uk

O. Ozioko
e-mail: O.Ozioko@derby.ac.uk

O. Bagdasar
School of Computing, University of Derby, Markeaton Street, Derby, UK
e-mail: O.Bagdasar@derby.ac.uk

Department of Mathematics, Faculty of Exact Sciences, 1 Decembrie 1918, University of Alba Iulia, 510009 Alba Iulia, Romania

T. O. Roy-Layinde
Department of Physics, Olabisi Onabanjo University, Ago-Iwoye, Ogun State, Nigeria
e-mail: roy-layinde.taiwo@oouagoiwoye.edu.ng

1 Introduction

Resonance is one of the interesting behaviours that low-order systems, modelled as nonlinear ordinary differential equations, are known to display. This behaviour leads to the creation of unusual attractors, and other phenomena, such as hysteresis and jump phenomenon, and period doubling bifurcation. The knowledge and interpretation of these behaviours, facilitates the understanding of the complex dynamics of various physical systems, and enables a straightforward analysis [1].

Resonance is one of the significant phenomena displayed by nonlinear systems, which is due to its ability to store and transfer energy, from an external driving source, as well as to provide a system's maximum response. While it is beneficial in some applications (e.g., communication, vibration therapy and medicine), it may also cause instability or even disastrous out-

Journal: 11071 MS: 10534 TYPESET DISK LE CP Disp.:2024/11/4 Pages: 21 Layout: Medium

comes in others, when not properly controlled [2]. Notable importance is given to resonances in biological sciences, physical sciences, and engineering. A system is said to be in resonance when its inherent vibration frequency, matches the frequency of an external driving force, thereby increasing the output response. [3,4].

Resonance has been defined more broadly to include all processes involving the optimisation, suppression, or amplification of a system's response by the modulation of any parameter of the system. Therefore, the restriction on solely frequency matching has been modified [4,5]. Resonance that occurs in a nonlinear system is referred to as nonlinear resonance. In this instance, frequency matching is not necessary for resonance to occur, unless specified design requirements are met [3]. When an external driving force is applied, a system's maximum response, at low frequency (LF), is enhanced. This phenomenon, known as nonlinear resonance, can take many different forms, depending on the type of driving force [2,4]. For instance, what is now known as vibrational resonance (VR), occurs when the force manifests as a high-frequency (HF) periodic signal [6,7]. In VR, a nonlinear system responds to a LF signal, in a resonant manner, when an ideal amplitude of HF stimulation is delivered to it. As a result, the effect of a HF excitation is comparable to that of noise, in the well-known stochastic resonance (SR) phenomena [8–10]. Additionally, several nonlinear systems, subjected to external energy sources and particular parameter settings, exhibit nonlinear resonance, termed parametric resonance [11,12]. Autoresonance, also known as self-sustained resonance, is the ability of a nonlinear oscillator to maintain resonance in the face of changes in its structural and/or excitation characteristics [3,4,13].

Vibrational resonance (VR) has generated significant scientific attention in the last two decades owing to its potential industrial applications. These are especially relevant to communications, signal identification, separation and extraction, noise attenuation, filtering, optimisation and control of signal output, and energy emphasis [4]. Other cutting-edge technological applications include ratchet-like components, such as nonlinear mixers, sensors, transducers, amplifiers, switches, and filters. When used in VR regimes, these components provide better efficiency and operating conditions [3,4]. Motivated by the previously indicated possible applications, VR has now been demonstrated and evaluated in a variety of model systems, theoretically [7], numerically [6], and experimentally [14]. These spanned through several fields, including neuroscience, plasma physics, laser physics, acoustics, and engineering. Recently, VR has specifically been investigated in a doubly unique mass distribution function position-dependent mass (PDM) oscillator, which characterises the vibrational inversion mode of the NH_3 molecules [15]. The research demonstrated how the variable mass parameters of the molecules affect the resonance characteristics of the system.

In addition, the phenomenon of vibrational resonance was investigated in a Rayleigh-Plesset oscillator, for a gas bubble oscillating in an incompressible liquid, excited by a dual-frequency acoustic force, consisting of high-frequency, amplitude-modulated, weak signal [16]. The authors, presented convincing proofs, that an acoustically-driven bubble oscillates in a time-dependent single- or double-well potential, the characteristics of which are dictated by the liquid's properties. Furthermore, their findings of multiple resonances and their origin for the double-well situation were reported, along with their relationship to the weak, low-frequency acoustic force field.

However, research on the occurrence of VR, in acoustic resonators, have been under-explored. It was observed that much attention have not been given to the occurrence of VR, in acoustic resonators. It should be noted that, in acoustical domains, viscoelastic materials, resonators, and porous materials (foams or multilayered systems), are a few examples of the various passive control techniques used for sound absorption, possibly because porous materials remain in viscous regimes, at lower frequencies. Moreover, they are typically more efficient at higher frequencies [17].

For example, metamaterials are customised for improved mechanical, acoustic, electrical or optical processes. To be specific, acoustic metamaterials are designed to control, direct, and manipulate sound waves in gases, liquids, and solids. They can be engineered to either transmit, or trap and amplify acoustic waves at specific frequencies. Several acoustic metamaterial (AMM) systems can be designed based on Helmholtz resonators (acoustic resonators), which are frequently employed, for sound absorption and amplification, at lower frequencies [18]. The Helmholtz resonator (HR) increases sound pressure level of an audio signal, at a particular frequency band, and then attenuates it at frequencies outside that band, thereby performing as a typical sound absorber. Additionally, acoustic cloaking [19,20], acoustic topological sys-

Journal: 11071 MS: 10534 TYPESET DISK LE CP Disp.:2024/11/4 Pages: 21 Layout: Medium

tems [21,22], sound focusing based on gradient index lenses [23,24], perfect absorbers [25,26], and others, are some of the developed applications of AMMs. The technology have benefited from the study of nonlinear dynamics, especially, the propagation of acoustic waves in a periodic waveguides [27–29]. The nonlinearities of acoustic metamaterials are important to consider, especially for cylindrical pipe-based metamaterials that have resonance phenomena in tubes or lattices and intensify nonlinear effects in limited spaces. Knowledge of the dynamics of nonlinear acoustic metamaterials, have yielded significant progress in modern engineering and some of its applications are utilized in, nonlinear acoustic superlens [30,31], acoustic diodes [32,33], photonics metamaterials [34], and acoustic switching and rectification [35].

The effect of high-amplitude sound wave propagation in an acoustic metamaterial was recently reported by Zhang et al. [36], demonstrating the system's potential usage as a nonlinear absorber. However, the authors noted that the propagation of nonlinear losses cannot be disregarded, when both the fundamental and the second harmonic are taken into account. Using the classical perturbation approach, Lan et al. [37], examined the nonlinear effects of acoustic wave propagation and dispersion in a cylindrical pipe containing periodically organised Helmholtz resonators. The analytical findings revealed a shift in the resonant frequency to the lower frequency side and a widening forbidden bandgap of the transmission spectrum, which were caused by the nonlinearity of the Helmholtz resonators and the increase in the incident acoustic pressure level. To overcome this, many authors studied the nonlinearities in the system's restoring force, to enable more effective vibration control across a wider frequency range [17,38,39].

More recently, nonlinear damping and nonlinear restoring force were proposed, to comprehend the dynamic behaviours of the acoustic resonator, and to significantly enhance the efficiency of HRs. Singh and Rienstra [40], modelled a HR with a linear restoring force and a nonlinear damping term, while in a recent publication, Forner et al. [41] described various kinds of dissipations that might occur in a HR. Both authors argue that vortex shedding is primarily responsible for the nonlinear dissipation, while thermo-viscous boundary layers are responsible for the linear dissipation. In other studies, the nonlinear damping, caused by the jet loss, and the nonlinear restoring force (a quadratic and cubic term), caused by the nonlinear elasticity of the cavity air, for large amplitude excitations, were both considered [17,42]. Vakakis [42] reported a slightly softening behaviour for the HR model. However, the work of Meissner [43], confirmed the dependence of the Helmholtz resonator's frequency on the flow velocity, the type of flow (turbulent or laminar), and the shape of the resonator. Additionally, Forner et al. [41] demonstrated that the geometry of the neck, might affect the appearance and dissipation of vortices, around the neck, and as well, play a vital role on the dynamical behaviour of the system. This implies that, if the vortex and dissipation around the neck are minimised, it is possible to investigate, further, in the nonlinear domain, while considering the nonlinear restoring force. Recently, Alamo Vargas et al. [17], developed a method to do this by modifying the neck geometry. In addition to the softening behaviour previously reported, the authors achieved a hardening behaviour, by limiting the vortex shedding, with a customised nonlinear HR neck. Consequently, the governing nonlinear equation, of the Helmholtz resonator, enabled the calculation of extreme nonlinear response behaviours, of the system.

In light of the aforementioned, we investigated and evaluated the VR phenomenon, in a bi-harmonically driven Helmholtz resonator, where, to the best of our knowledge, the influence of a high-frequency excitation (auxiliary signal) on a weakly driven HR, has not yet been addressed. In VR, a second high-frequency harmonic, referred to as the fast-signal, usually stimulates a nonlinear system driven by a low-frequency signal, such that the high-frequency component, Ω, has a fundamental higher frequency value, compared to the low-frequency component, ω. The system's response amplitude, at the slow oscillation frequency, under these conditions ($\omega \ll \Omega$), is computed as a function of the amplitude of the high-frequency signal. Consequently, the response exhibits a curve akin to that of the well-known response of signal-to-noise ratio, found in stochastic resonance (SR) [8,44].

The paper is structured as follows: Firstly, the HR model, and its governing equation, are introduced in the next section (Sect. 2). Section 3 discusses the numerical simulations and the description of vibrational resonance phenomenon. Section 4 contains the results and discussions of our findings. Lastly, in Sect. 5, we summarise the paper and conclude, with brief discussions on some important applications of our findings.

Journal: 11071 MS: 10534 TYPESET DISK LE CP Disp.:2024/11/4 Pages: 21 Layout: Medium

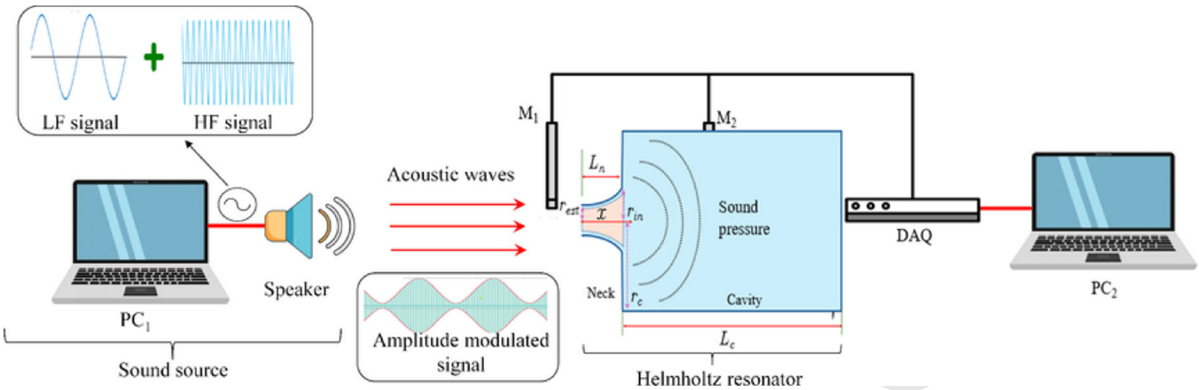

Fig. 1 A simple description of the HR unit, driven by amplitude modulated acoustic waves, and a schematic of the system's behaviour with the displacement of air molecules, along the tailored neck of the resonator

2 Model description

To study the occurrence of VR in an acoustic resonator, we utilised a HR, the mechanical system shown in Fig. 1. This is because of its characteristic nonlinearities. Moreover, to promote the application of acoustic resonators, there is a need to investigate the resonance dynamics, of the system, in the nonlinear regimes. The effect of sound pressure level, which is the varying amplitude of the driving force, was investigated, using the response behaviour of the system, in [17]. In this paper, we assumed that the acoustic force is weak, and it is amplitude-modulated. However, it is worth mentioning that, in response to the incident acoustic pressure across the resonator's opening, its resonant frequency is determined by the dimension of its cavity volume and neck area. Therefore, L_n and L_c are the length of the neck and cavity, respectively, while V_0 is the volume of the HR cavity. The external and internal radii of the hyperboloid neck are r_{ext} and r_{in}, respectively, and r_c is the radius of the cavity. These parameters were utilised for the derivation of a dimensionless equation. In the long wave limit, the air inside the cavity is considered as a nonlinear spring, so that the change in pressure (Δp), resulting from the displacement z of air in the neck can be written as

$$\Delta p = -\upsilon \left(z - \frac{(\gamma+1)S}{2V_0} z^2 + \frac{(\gamma+1)(\gamma+2)S^2}{6V_0} z^3 \right), \tag{1}$$

where $\upsilon = \rho \omega_0^2 L_{eff}$ and ρ (kg/m^3) is the air density. L_{eff} (m) is the effective length of the neck and ω_0 (s^{-1}) is the linear resonance frequency of the resonator, which depends on the cross sectional area, S (m^2) of the neck and volume, V_0 (m^3) of the cavity. γ is the specific heat ratio of air, such that combining the momentum equation and the nonlinear restoring force, with the nonlinear damping and the external pressure increment, the equation of motion with respect to time τ (s), takes the form [17],

$$\frac{d^2 z}{d\tau^2} + \left(\frac{\eta}{2L_{eff}} \right) \frac{dz}{d\tau} \left| \frac{dz}{d\tau} \right| + \left(\frac{\mu S}{\rho L_{eff}} \right) \frac{dz}{d\tau} + \omega_0^2 z - \left(\frac{\alpha S \omega_0^2}{V_0} \right) z^2 + \left(\frac{\beta S^2 \omega_0^2}{V_0^2} \right) z^3 = -\frac{p^*}{\rho L_{eff}}, \tag{2}$$

where η is the coefficient of the total hydraulic resistance of the neck, and μ (Ns/m^5) accounts for the sum of the acoustic impedance at the inlet of the HR and the friction acoustic impedance. $\alpha = \frac{(\gamma+1)}{2}$, $\beta = \frac{(\gamma+1)(\gamma+2)}{6}$, and p^* (N/m^2) is the pressure variation around the atmospheric pressure. By re-scaling the variables in Eq. (2) as

$$t = \omega_0 \tau, \quad x = \frac{Sz}{V_0}, \quad \sigma = \frac{\eta V_0}{2SL_{eff}} \quad \text{and} \quad \delta = \frac{\mu S}{\rho \omega_0 L_{eff}}, \tag{3}$$

the nonlinear equation, for the motion of air molecules passing through the neck into the HR's cavity, driven by an external acoustic excitation, is described in terms

Journal: 11071 MS: 10534 TYPESET DISK LE CP Disp.:2024/11/4 Pages: 21 Layout: Medium

of a dimensionless displacement, x, given as

$$\ddot{x} + \sigma \dot{x}|\dot{x}| + \delta \dot{x} + \frac{V(x)}{dx} = p, \tag{4}$$

where

$$\frac{V(x)}{dx} = x - \alpha x^2 + \beta x^3. \tag{5}$$

The external acoustic excitation, p ($p = \frac{Sp^*}{\rho V_0 \omega_0^2 L_{eff}}$), determines the system's response behaviour. In Eq. (4), σ is the nonlinear damping term, due to the jet phenomenon, while δ represents the linear damping. At low sound pressure levels, the nonlinear damping, can typically be ignored; however, at high sound pressure levels, σ, which is proportional to the ratio of cavity to neck volume, must be present [17]. Generally, a restoring force is created when the air in the cavity is compressed, and damping will be produced by the friction in the neck, caused by the fast-moving air. Various dynamic reactions, result from distinct orderings of the system's parameters. When the driving pressure is very low, the linear damping term predominates, and the contribution of the nonlinear restoration term, can be negligible. Hence, the motion of air molecules, in the neck, is reduced to linear vibrations, with linear damping (δ) only [40,42].

The integration of Eq. (5), gives the expression for the system's potential,

$$V(x) = \frac{1}{2}x^2 - \frac{1}{3}\alpha x^3 + \frac{1}{4}\beta x^4. \tag{6}$$

Here, the potential parameters, α and β, are dependent on the specific heat ratio of air, γ, which describes the thermodynamic state of the air molecules. Note that, the specific heat ratio of a gas is the ratio of the specific heat of the gas, at constant pressure, to its specific heat, at a constant volume [17]. The specific heat ratio of the air molecules in the neck, is a function of the excitation frequency of the acoustic wave, and the nature of air molecules. Generally, if the driving frequency is significantly high, the process becomes adiabatic, due to increasing temperature gradient, in the cavity. However, with a low driving frequency, the process becomes isothermal [16,17]. Therefore, an intermediate value for the specific heat ratio, $\gamma = 1.4$, can be used, which appropriately describes the thermodynamic state, of the air molecules, across the neck and in the cavity. Consequently, the estimated values, for the potential parameters, are $\alpha = 1.20$ and $\beta = 1.36$, as obtained experimentally in [17]. Thus, for this study, these values are fixed for the associated parameters, throughout our analyses, apart from the potential plots in Fig. 2. Additionally, the values for both linear and nonlinear damping terms, $\delta = 0.005$ and $\sigma = 0.05$, respectively, are fixed as well, except otherwise indicated.

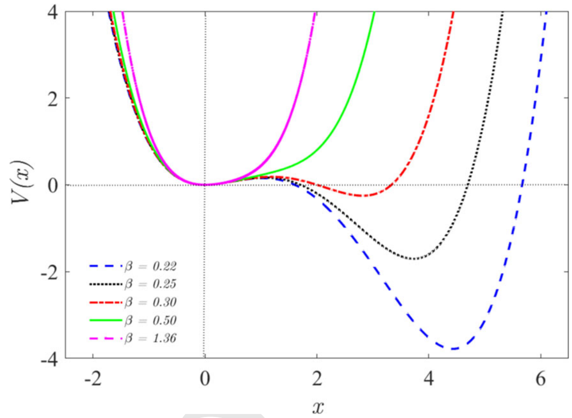

Fig. 2 The potential structure of the system with $\alpha = 1.2$ and $\beta = [0.22, 0.25, 0.30, 0.50, 1.36]$

The system's potential structure is shown in Fig. 2, for different values of β ($\beta = [0.22, 0.25, 0.30, 0.50, 1.36]$), with fixed value of α ($\alpha = 1.2$). It is clear that the system exhibits a single-well potential structure with $\beta = 1.36$, which implies that the system posses only one equilibrium point, $x = 0$, for the parameter setting. However, the system can also admit additional equilibrium points, depending on the choice of β. For instance, it exhibits three equilibrium points, two stable equilibria and an unstable equilibrium, a typical asymmetric double-well-single-hump potential structure, when $\alpha^2 - 4\beta > 0$. The potential plots satisfying this condition, is shown in Fig. 2, with a dash line, a dotted line and a dash-dotted line, for $\beta = 0.22, 0.25$ and 0.30, respectively.

3 Numerical simulations and the description of VR

It is worth mentioning that the dynamic regimes of the HR model, can vary greatly, as a function of the system's parameters of interest. Moreover, the experimental results of Alamo Vargas et al. [17], limits the value of the system's parameters. This appears logical and very realistic, physically. Hence, to investigate the occurrence of VR, with the modelled nonlinear equation, system (4) is assumed to be under the influence

Journal: 11071 MS: 10534 TYPESET DISK LE CP Disp.:2024/11/4 Pages: 21 Layout: Medium

of an amplitude-modulated acoustic excitation, $p = A\cos\omega t$. This is such that, A ($A = (g\cos\Omega t + f)$), is the amplitude of the acoustic wave, comprising; the amplitude of a weak low-frequency (LF) signal, f, modulated by a cosine signal, $g\cos\Omega t$, which is a high-frequency (HF) periodic signal. It should be noted that, ω represents the low-frequency parameter, while g and Ω, are the amplitude and frequency of the high-frequency acoustic perturbation. In Fig. 1, we presented a well-labelled schematic, for the purpose of implementation. The amplitude modulated acoustic waves can be achieved by connecting a speaker, to an amplifier or directly, to a computer unit, PC_1, as shown on the left-hand side of the figure (Fig. 1). Microphones, M_1 and M_2, can be positioned with the resonator (Fig. 1), to measure the input and output sound pressure level, respectively. Data from both microphones could be logged by connecting them to a computer (PC_2), via a data acquisition device, DAQ.

Substituting for p, and $\frac{dV(x)}{dx}$ from Eq. (5), in Eq. (4), the modelled nonlinear HR equation can be written as

$$\left.\begin{aligned} \ddot{x} \;+\; & \sigma\dot{x}|\dot{x}| + \delta\dot{x} + x - \alpha x^2 + \beta x^3 \\ = \; & (g\cos\Omega t + f)\cos\omega t, \end{aligned}\right\} \tag{7}$$

which facilitate the occurrence of VR. Furthermore, we have chosen, for convenience, $\Omega \gg \omega$, as the respective frequencies, a condition that must be satisfied, for the VR occurrence. Hence, Eq. (7) can be rewritten as a set of coupled first-order Ordinary Differential Equations (ODEs) of the form

$$\left.\begin{aligned} \frac{dx}{dt} &= \dot{x} \\ \frac{d\dot{x}}{dt} &= -\sigma\dot{x}|\dot{x}| - \delta\dot{x} - x + \alpha x^2 - \beta x^3 \\ &+ (g\cos\Omega t + f)\cos\omega t. \end{aligned}\right\} \tag{8}$$

Equation (8) was integrated, using the Fourth-Order Runge-Kutta scheme, with a fixed step size, $\Delta t = 0.001$. Considering zero initial conditions, that is $x(t) = 0$ and $\dot{x}(t) = 0$, and using the output signal's time series, of Fourier sine and cosine components, A_S and A_C, respectively, the response amplitude, Q can be calculated from

$$\left.\begin{aligned} Q &= \frac{\sqrt{A_S^2 + A_C^2}}{f} \\ \theta &= -\tan^{-1}\left(\frac{A_S}{A_C}\right), \end{aligned}\right\} \tag{9}$$

where,

$$\left.\begin{aligned} A_S &= \frac{2}{nT}\int_0^{nT} x(t)\sin\omega t\, dt, \\ A_C &= \frac{2}{nT}\int_0^{nT} x(t)\cos\omega t\, dt. \end{aligned}\right\} \tag{10}$$

The period of oscillation, of the low-frequency input signal, $T = \frac{2\pi}{\omega}$, with $n = [1, 2, 3, \ldots]$, number of complete oscillations.

4 Result and discussion

4.1 Trajectory of the system's particles

To analyse the response behaviour of system 7, firstly, we studied the dynamics of its particles. It should be noted that in many cases, chaotic dynamics can be seen in certain parameter regimes, for many forms of nonlinear systems, especially oscillators with quadratic or higher order polynomial potentials. To understand this, the bifurcation diagrams of the system's dynamics, is presented, with increasing values of f, the amplitude of the LF signal, when the fast signal is yet to be activated ($g = 0$). This is shown in Fig. 3a. It is evident, from the figure, that the possibility of chaos increases with higher values of f. A previous work had reported the possibility of chaos, when homoclinic orbits ceased to exist [17]. However, a periodic regime is observed for small forcing amplitudes, $0 < f \leq 2$, as shown in Fig. 3a. Next, we present the bifurcation diagram of the system presented in Eq. (7), with varying low-frequency, ω, values, when $f = 1.0$ and $g = 0.0$, in Fig. 3b. Other system parameters are fixed at $\alpha = 1.2$, $\beta = 1.36$, $\sigma = 0.05$, and $\delta = 0.005$. The figure (Fig. 3b), facilitates an explicit knowledge of the significance of ω, on the system's dynamics. Thus, it paves the way for a better understanding of the significant influence of frequency, on the theories and concept of the resonance behaviour of the system, particularly, the fundamental changes the air molecules in the HR cavity, under goes.

Clearly, the system of Eq. (7), presents three distinct behaviours, as the frequency, ω increases. *Stage I*, the start-up regime, with a chaotic dynamics in the range, $0 < \omega < 0.95$. *Stage II*, is the highly controllable regime, with the air molecules in a periodic motion, for $0.95 \leq \omega \leq 1.60$. However, in *stage III*, the main significant feature of the system is the period-

Journal: 11071 MS: 10534 TYPESET DISK LE CP Disp.:2024/11/4 Pages: 21 Layout: Medium

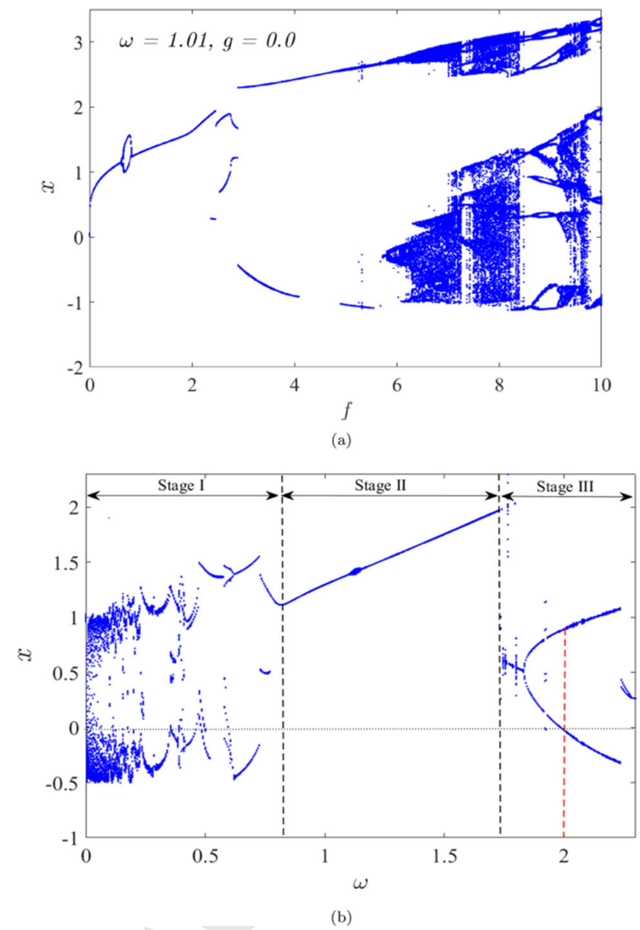

Fig. 3 Bifurcation diagram of the HR system with, **a** increasing low-frequency amplitude, f, when the amplitude of the fast signal, $g = 0$. Other system parameters are $\alpha = 1.2$, $\beta = 1.36$ and $\omega = 1.01$, $\sigma = 0.05$, $\delta = 0.005$; **b** increasing low-frequency component, ω, while $f = 1.0$ and $g = 0.0$. Other system parameters are $\alpha = 1.2$, $\beta = 1.36$, $\sigma = 0.05$, $\delta = 0.005$

doubling bifurcation, at $\omega = 2.0$. The periodic window (*stage II*), which only exist for a small range of the LF component (ω), appears reasonable and very realistic. This is because typical HRs, exhibit a single resonant frequency. Additionally, improving the resonance behaviour in this regime, is the crux of this research findings. It should be noted, that the dynamics of the HR, is highly chaotic, and a fundamental feature of most complex dynamical systems, is their sensitivity to initial conditions, and sets of parameter values [45,46]. These observable features can be utilised in different field applications of the HR. In essence, the bifurcation diagram offers a thorough and visual representation of the complex dynamics of the system, influenced by the frequency fluctuations. Thus, it summarises the completeness of our investigations, in this paper. Moreover, one of the novelty of our findings is its ability to predict motions of the air molecules in the cavity at each stage (*stage I, stage II* or *stage III*), and their resultant effect on the observed phenomenon (VR).

To fully comprehend the behaviour of the system, the motion of the air molecules, in Fig. 4, was examined, for four different values of the amplitude of the LF acoustic wave, f. The phase portraits and the corresponding trajectory plots, are shown in Fig. 4a and b, respectively. In Fig. 4a(i), the motion is highly periodic. Further increase in the value of f, leads to a multi-periodic orbit, showcased in Fig. 4a(ii), and a quasi-periodic motion, in Fig. 4a(iii). However, with $f = 7$, a chaotic attractor emerges.

Although the attractor adopts a pattern akin to that reported by Alamo Vargas et al. [17] (see Fig. 8a of [17]), when $f \leq 0.4$, shown in Fig. 6, the observed dynamics is distinct, particularly, for $f > 0.4$. It is worth mentioning that, both Fig. 3a and b, show the rich bifurcation scenarios of the system, with changing parameters of the LF acoustic signal and their relation-

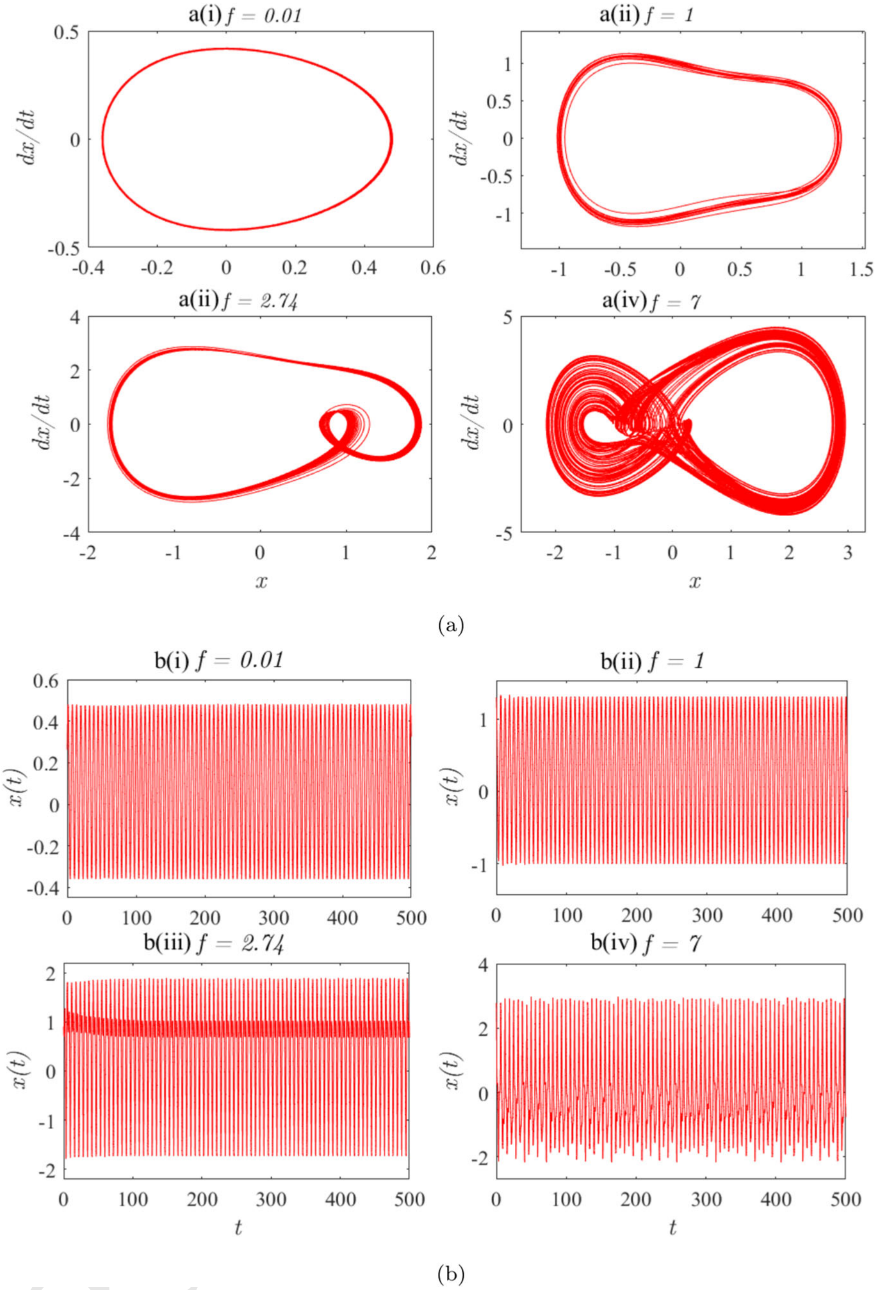

Fig. 4 **a** Phase portraits of the HR system, before the activation of the fast signal ($g = 0$), for different values of LF amplitude; (i) $f = 0.01$, (ii) $f = 1.0$, (iii) $f = 2.74$, and (iv) $f = 7.0$; **b** The corresponding time-series plots. Other system parameters are $\omega = 1.01$, $\sigma = 0.05$, $\delta = 0.005$, $\alpha = 1.2$, $\beta = 1.36$

ship to particle transport, as depicted with phase portraits and evolution plots. They all present the typical chaotic behaviour of the HR model, showing the dependence of the particle's motion on the acoustic signal. This, consequently, shows that asides the previously reported softening and hardening behaviours, the system can display other dynamics, due to the significant impact of the acoustic pressure on the air molecules. Therefore, one would be curious to know if the signature will persist, on the air particles, at different frequencies, or if other behaviours would appear, due to frequency variations. This constitutes one of the major focus of this work; to examine the significance of frequency change, on the dynamics of the HR.

To gain deeper insight into the dynamics of the system, when subjected to an acoustic signal, we turn our

Journal: **11071** MS: **10534** TYPESET DISK LE CP Disp.:**2024/11/4** Pages: **21** Layout: **Medium**

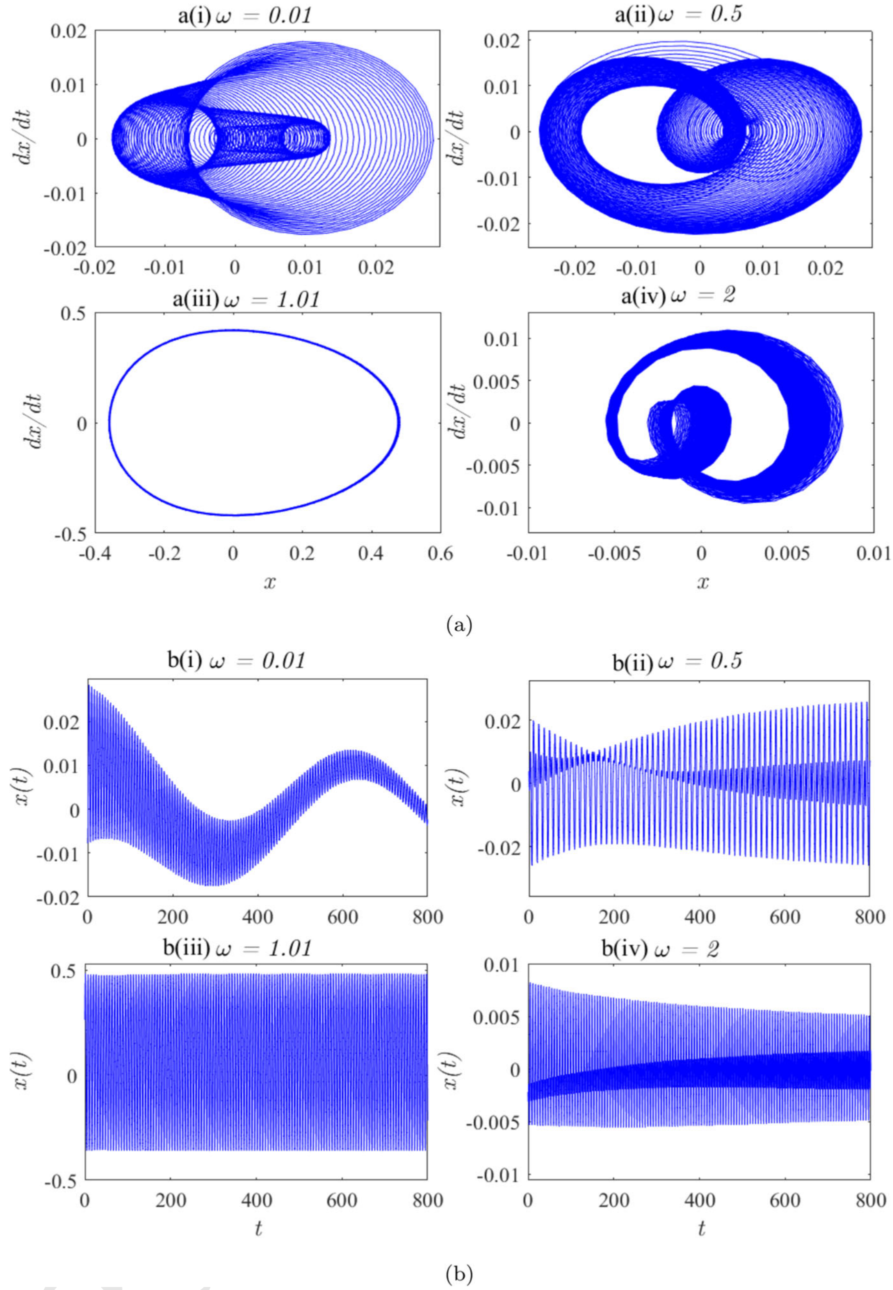

Fig. 5 **a** Phase portraits of the HR system, before the activation of the fast signal ($g = 0$), for different values of the low-frequency component; (i) $\omega = 0.01$, (ii) $\omega = 0.5$, (iii) $\omega = 1.01$, and (iv) $\omega = 2.0$; **b** The corresponding time-series plots. Other system parameters are $f = 0.01, \alpha = 1.2, \beta = 1.36, \sigma = 0.05, \delta = 0.005$

attention to the alteration of the phase diagram, in the periodic regime (Fig. 4a(i)). This is achieved by adjusting the LF component, ω. The exploration is showcased in Fig. 5a, where the phase portraits are presented for four different values of ω ($\omega = [0.01, 0.5, 1.01, 2.0]$). To the best of the authors' knowledge, no prior research, in the field of acoustics, has examined the intriguing behaviours, displayed by the numerical simulations of Eq. (7), shown in Fig. 5a and 5b. Conspicuously, with $\omega = 0.01$ in Fig. 5a(i), the trajectory is novel, despite its chaotic nature. It is very logical to assume that the consequence of different transformations, inside the acoustic resonator, results to the horn-shaped trajectory. Note, in an ideal HR, the air molecules inside the cavity, which are considered compressible, move freely [17,40,42]. However, the air column in the neck,

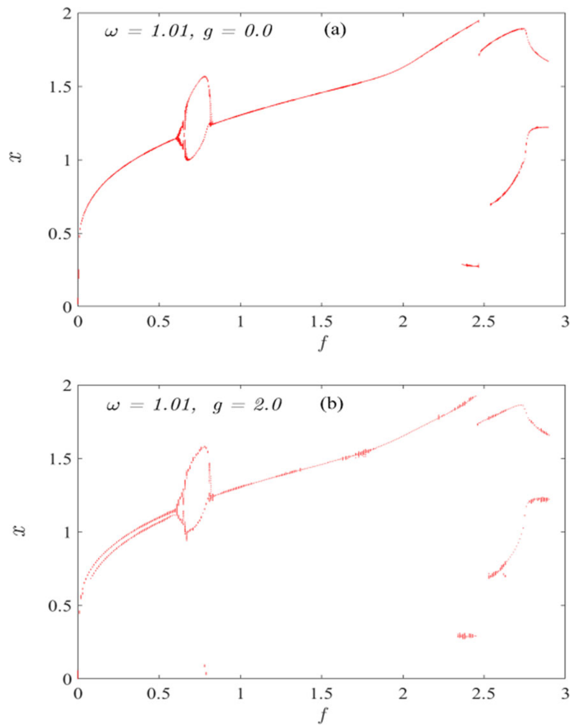

Fig. 6 Bifurcation diagram within a small range of the LF amplitude, $f \in (0, 3)$, for **a** $\omega = 1.01$ and $g = 0$, while other parameters were fixed at $\alpha = 1.2$, $\beta = 1.36$, $\Omega = 0.0$, $\sigma = 0.05$, $\delta = 0.005$; **b** $\omega = 1.01$ and $g = 2.0$, while other parameters were fixed at $\alpha = 1.2$, $\beta = 1.36$, $\Omega = 10\omega$, $\sigma = 0.05$, $\delta = 0.005$

which is regarded as an incompressible mass, can only oscillate narrowly towards the neck end, and eventually diffuse into the cavity, due to the acoustic pressure. Increasing the frequency, $\omega = 0.5$ in Fig. 5a(ii), the air molecules vibrate conically, and oscillate periodically when $\omega = 1.01$ in Fig. 5a(iii). However, there is a significant decrease in oscillation amplitude, beyond the periodic regime ($\omega = 2.0$), as shown in Fig. 5a(iv). These are also captured by the corresponding trajectory plots, in Fig. 5b(i)–(iv).

To gain further insight into the behaviour the system, especially, the effect of the HF signal, on the dynamics of the HR, we present the bifurcation diagrams, within a small range of the LF amplitude, $f \in (0, 3)$, in Fig. 6a and b. Presented in Fig. 6a, is the bifurcation diagram without activating the HF signal, $g = 0.0$. On the other hand, Fig. 6b, depicts the effect of the HF acoustic signal, on the system's dynamics. For both figures, other system parameters are fixed at $\alpha = 1.2, \beta = 1.36, \Omega = 10\omega, \sigma = 0.05$, and $\delta = 0.005$. Although both figures look very alike, they are required to unveil the intricate behaviour of the system. This stems from the fact that, it appears difficult to discern some patterns in Figs. 3a and 6a. Moreover, the scenario of the system, subjected to a HF signal, as shown in Fig. 6b, revealed different array of dynamics, that include periodic, multi-periodic motion, bifurcation bubble, reverse period doubling, and even chaotic motions, as f increases. In another words, the periodic regime is distinguishable with the activation of the HF signal. This facilitates the selection of the appropriate choice of the LF amplitude, f, which, successfully, enhanced the system's performance, by modulating the parameters of the HF signal.

Next, we examined the possible effect of the HF signal, on the dynamics of the system. For four distinct values of the LF component, similar to Fig. 5a, we studied the behaviour of the system and noted the significant changes in the trajectories. This is shown in Figs. 7a(i)–(iv) and b(i)–(iv). Notably, the chaotic behaviours of the air molecules, are suppressed. Additionally, the system sustained a periodic dynamics, with $\omega = 1.01$, shown in Fig. 7a(iii), and a quasi-periodic motion, when $\omega = 2.0$, as shown in Fig. 7a(iv). The corresponding time evolution, for these trajectories, are shown in Fig. 7b(i)–(iv).

4.2 Acoustic vibrational resonance

It is evident that the system's dynamics is chaotic and highly complex. Additionally, we observed that the type of application and the environmental condition, determine the geometry and size of some fundamental parameters, like the length and cross-sectional area of the neck, volume of the cavity, the total hydraulic resistance, and acoustic impedance, at the inlet of the HR. More so, the nonlinear damping σ, caused by the jet phenomenon, is a function of the hydraulic resistance, and is proportional to the ratio of the cavity volume to that of the neck [17,42]. For the purpose of examining the nonlinear response of the system, the effect of restoring and damping forces, were also considered, in addition to the influence of the acoustic field. The air inside a resonator's cavity is primarily where the nonlinear restoring force comes from, which is seen as a nonlinear spring in the long wave limit [42].

First, the frequency response curve of system (7), in Fig. 8, is examined. The system's response curve for different values of the HF component, $\Omega =$

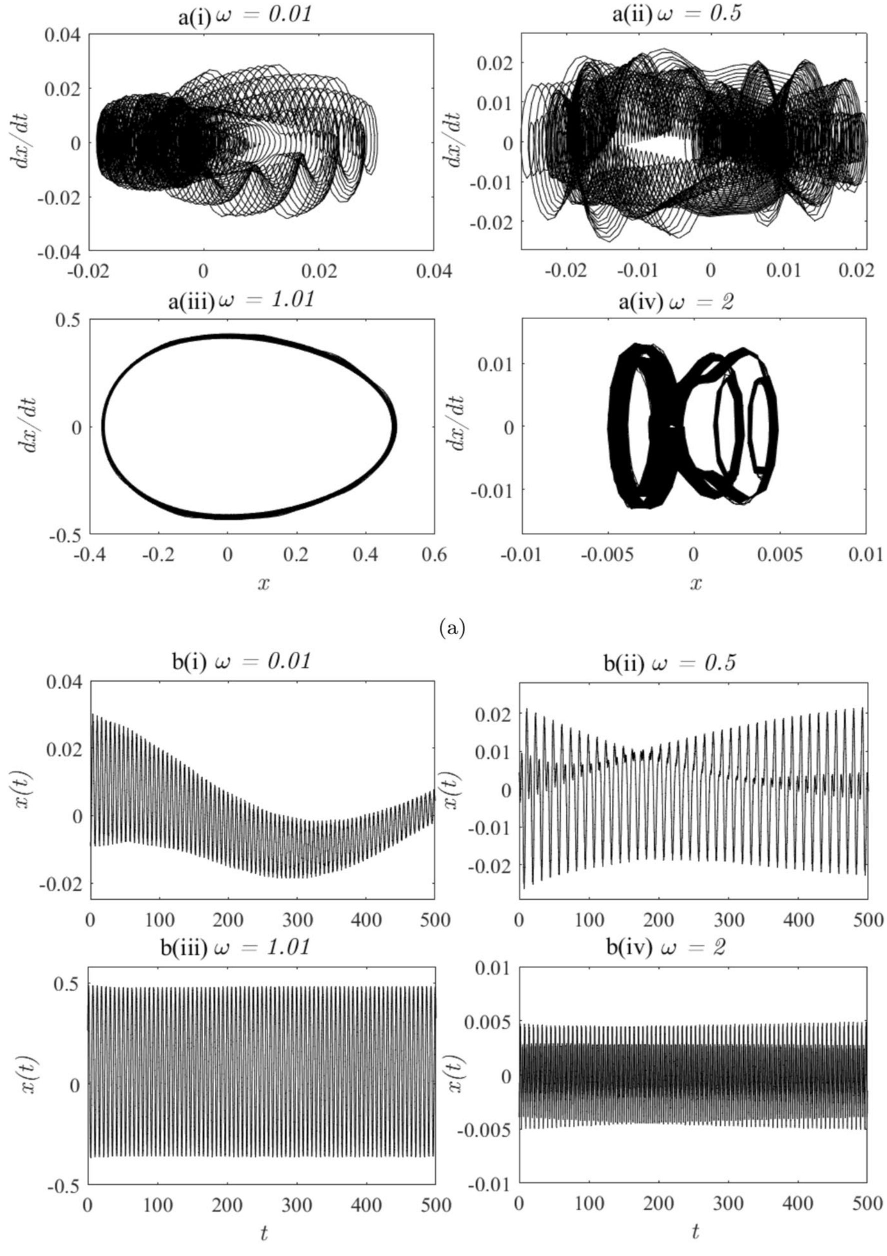

Fig. 7 **a** Phase portraits of the system with $g = 0.1$, for four values of the low-frequency component; (i) $\omega = 0.01$, (ii) $\omega = 0.5$, (iii) $\omega = 1.01$, and (iv) $\omega = 2.0$; **b** The corresponding time-series plots, while other system parameters are $f = 0.01, \sigma = 0.05, \delta = 0.005, \alpha = 1.2, \beta = 1.36$ and $\Omega = 10$

[8.0, 9.0, 10.0, 11.0], when the amplitude of the HF signal, $g = 1.0$, is shown in Fig. 8a. However, Fig. 8b, depicts the response when the HF acoustic signal is not activated. It is clear, from Fig. 8a, that, aside the main response curve, observed at $\omega = 1$, for the considered values of Ω, it is possible to have harmonics at higher ω, when the HF signal is activated. Next, the effect of varying the amplitude of the LF acoustic signal, f, on the system's response, in Fig. 9, is presented. The response curves, for different values of f ($f = [0.01, 0.05, 0.083]$), are shown in Fig. 9a, while Fig. 9b presents a similar effect, for high pressure amplitude, $f = [1.0, 1.7, 2.74]$. Other system parameters were fixed at $g = 1.0, \alpha = 1.2, \beta = 1.36, \Omega = 10, \sigma = 0.05$ and $\delta = 0.005$. It is evident that the system responds, significantly, to the chang-

Journal: 11071 MS: 10534 TYPESET DISK LE CP Disp.:2024/11/4 Pages: 21 Layout: Medium

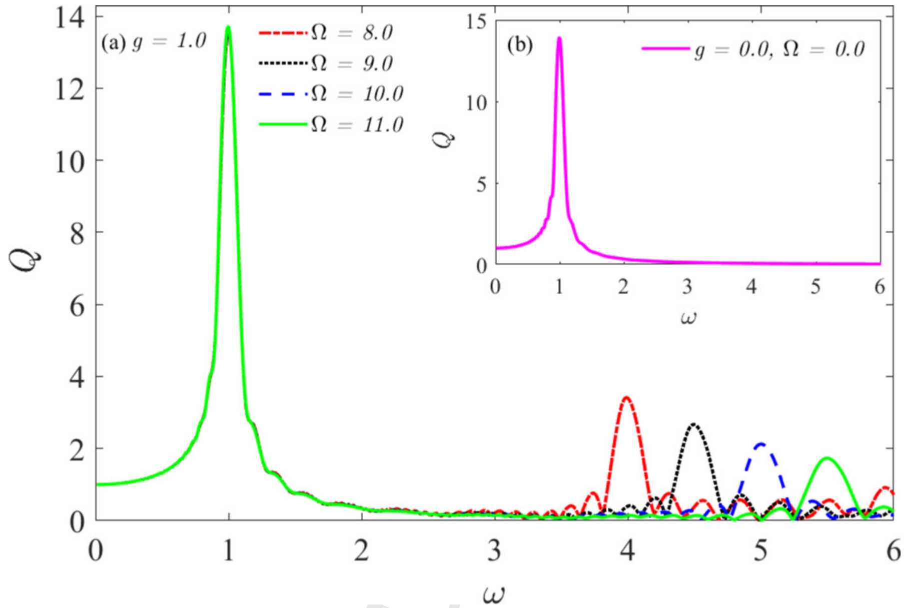

Fig. 8 **a** The system's frequency response curve for different values of the HF component, $\Omega = [8.0, 9.0, 10.0, 11.0]$, when the amplitude of the HF signal, $g = 1.0$. **b** Frequency response curve in the absence of the HF signal, $g = 0.0$, $\Omega = 0.0$. Other parameters of the system were fixed at $f = 0.01$, $\alpha = 1.2$, $\beta = 1.36$, $\omega = 1.01$, $\sigma = 0.05$ and $\delta = 0.005$

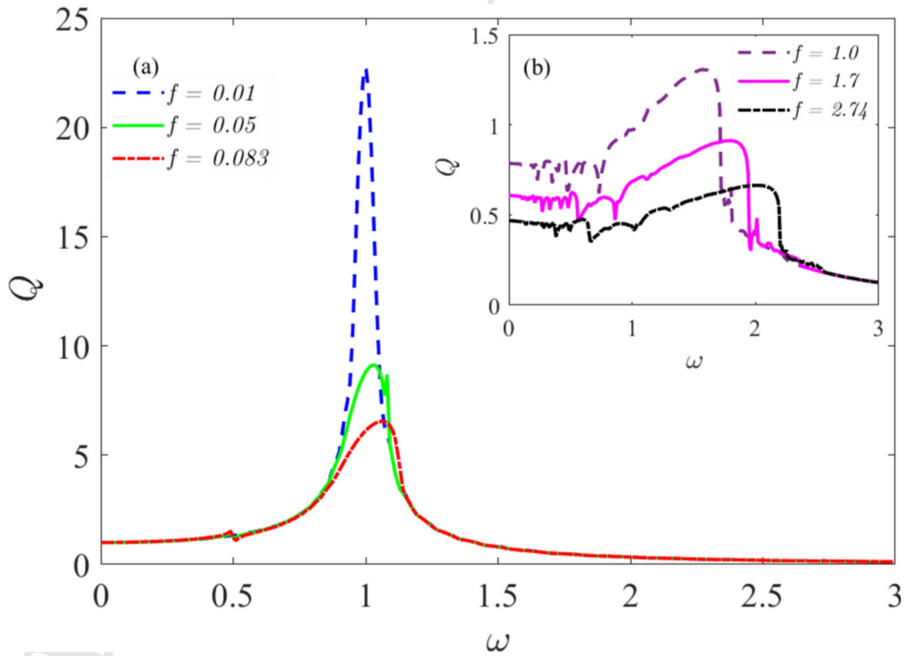

Fig. 9 Frequency response curves, for different values of the amplitude of the LF signal; **a** $f = [0.01, 0.05, 0.083]$, and **b** $f = [1.0, 1.7, 2.74]$. Other system parameters are $g = 1.0$, $\alpha = 1.2$, $\beta = 1.36$, $\Omega = 10$, $\sigma = 0.05$, and $\delta = 0.005$

ing values of the acoustic wave amplitude. Increasing f, reduces the response amplitude, and shifts the resonant frequency to the right. This is a hardening stiffness behaviour, which has been studied in literature. For instance, Alamo Vargas et al. [17] examined the behaviour of the system (Eq. (7)) with $g = 0$, both experimentally and analytically, and reported that the system exhibited a softening behaviour, at low excitation amplitudes. Additionally, it was stated that the resonance frequency decreased with increasing amplitude. However, when the system's excitation level increased, the softening characteristic changed to a hardening behaviour. Consequently, the tendency that a system would exhibit a hardening behaviour, increases with

Journal: 11071 MS: 10534 TYPESET DISK LE CP Disp.:2024/11/4 Pages: 21 Layout: Medium

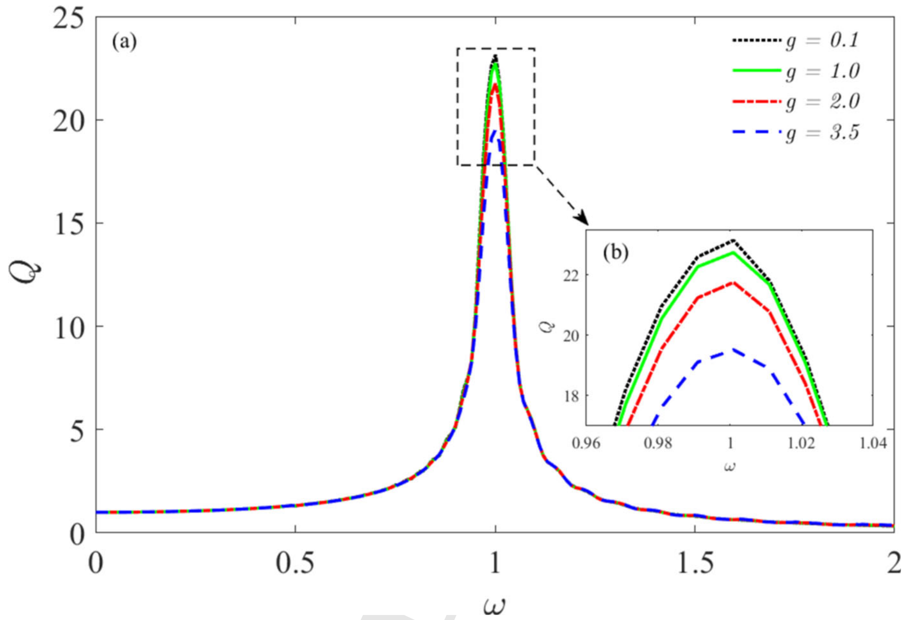

Fig. 10 The system's response curves, for different values of the amplitude of the HF signal; **a** $g = [0.1, 1.0, 2.0, 3.5]$, and **b** the insert of response peaks. Other system parameters are $f = 0.01, \alpha = 1.2, \beta = 1.36, \Omega = 10, \sigma = 0.05$ and $\delta = 0.005$

high amplitude excitations. Evidently, the characteristic hardening behaviour is captured in Fig. 9a, particularly, when $f > 0.05$, shown in Fig. 9b. To fully comprehend this, $f = 0.083,\ 1.70$ and 2.74, are the corresponding values of the sound pressure level (SPL), 89.3, 115.6 and 119.7 dB, respectively, which are realistically high [17,41].

In Fig. 10, the effect of amplitude of the HF signal, g, on the system's frequency response, was presented. Increasing g, reduces the systems response, as shown in Fig. 10a. This becomes obvious in Fig. 10b, an insert of the zoomed portion of the system's response curves. Similarly, the significant impact of both linear and nonlinear damping terms, δ and σ, is to decrease Q, the system's response, shown in Fig. 11a and b, respectively.

Now, we return to the main focus of this paper; to investigate the occurrence of VR in system (7). Next, the results obtained for the traditional VR phenomenon, are presented. It was shown that the air molecules, enclosed in the cavity of a resonator, described by system (7), undergoes VR through the dependence of the response amplitude, Q, on the HF amplitude, g, as shown in the following figures.
To emphasis the significance of investigating the occurrence of VR and reflect the impact of the HF signal, on the system's response, we define a gain factor, G_{VR} as

$$G_{VR} = \frac{Q_g(\omega)}{Q_0(\omega)}, \tag{11}$$

where, $Q_g(\omega)$ and $Q_0(\omega)$ are the response amplitude at the LF, ω, in the presence and absence of the HF signal, respectively. Variation of the gain factor, G_{VR} with increasing values of g, for different LF component, $\omega = [1.01, 1.05, 1.10]$, is shown in Fig. 12a. It is clear from the figure, that the quality of the system's response is improved, and with the appropriate choice of ω, a desired amplification can be achieved. The maximum gain and the corresponding value of the HF amplitude $(g, G_{VR_{max}})$, for the plotted values of the LF component, $\omega = 1.01, 1.05$ and 1.10, are (17.5, 1.18), (20.0, 2.33) and (23.0, 6.67), respectively. For instance, with a specified value of ω, the response amplitude can be controlled by modulating g. The fact that HR can absorb and amplify acoustic pressure at a particular frequency, determined by its dimension, shows that the size and geometry of the resonator dictates its response dynamics. Otherwise, at resonance, $\omega = \omega_r$. The resonant frequency, ω_r, is calculated from the cross-sectional area of the HR's neck and the volume of its cavity [47,48].

In Fig. 12b, the variation of Q with increasing values of the HF amplitude, g, for four different values of the LF component, ω ($\omega = [1.01, 1.05, 1.10, 1.25]$), is shown. Other system parameters are fixed at $f = 0.01, \Omega = 6.5, \alpha = 1.2, \beta = 1.36, \sigma = 0.05$, and $\delta = 0.005$. It is observed that the system's response, Q, increases with increasing values of ω. The con-

Journal: 11071 MS: 10534 TYPESET DISK LE CP Disp.:2024/11/4 Pages: 21 Layout: Medium

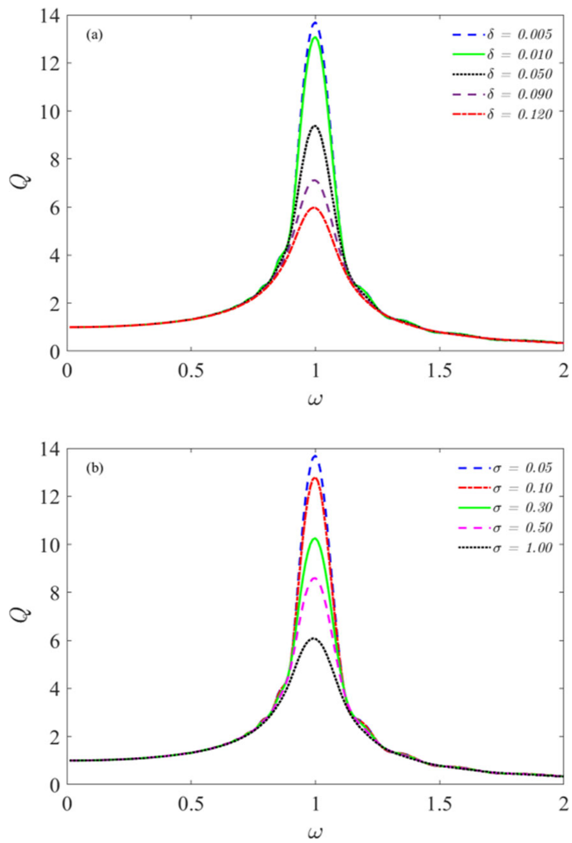

Fig. 11 The system's response curve for; **a** five different values of the linear damping parameter, $\delta = [0.005, 0.010, 0.050, 0.090, 0.120]$, with $\sigma = 0.05$; and, **b** five distinct values of the nonlinear damping parameter, $\sigma = [0.05, 0.10, 0.30, 0.50, 1.00]$, with $\delta = 0.005$. Other system parameters were fixed at $f = 0.01, \alpha = 1.2, \beta = 1.36, \omega = 1.01$, and $\Omega = 10$

tribution of the LF parameter, to the observed resonance behaviour, is clear from the figure (Fig. 12b), through the position of the peaks. Also, a double-peak resonance curve emerges, when $\omega = 2.0$, as shown in Fig. 12c. In Fig. 13, the dependence of the system's response, Q, on the HF amplitude, g, for six different values of the HF component, Ω ($\Omega = [6.5, 7.0, 7.5, 8.0, 8.5, 9.0]$), is presented, with other parameters of the system fixed at $f = 0.01, \omega = 1.01, \alpha = 1.2, \beta = 1.36, \sigma = 0.05$, and $\delta = 0.005$. Increasing Ω produced obvious changes in the maximum response; decreased Q, and also shifted the peak point towards higher values of g. As earlier mentioned, the LF component of the acoustic excitation, ω, imposes three distinct regimes of influence, on the dynamics of the system; (i) chaotic, (ii) periodic, and (iii) period-doubling, as depicted by Fig. 3b. Interestingly, their impacts, on the occurrence of VR, are examined, by varying the LF amplitude, f, in Fig. 14.

The effect of increasing the acoustic pressure amplitude, on the observed resonance phenomenon, is insignificant, when the particles exhibit choatic motions ($\omega = 0.01$), as shown in Fig. 14a. On the contrary, with an increased LF component ($\omega = 1.01$), shown in Fig. 14b, the system's response, Q, is well-enhanced, and can be meaningfully controlled by adjusting f, the pressure amplitude. Although, the maximum response amplitude, Q_{max}, decreases as f increases in Fig. 14b. By contrast, the cases reported in Fig. 14a, corresponding to $\omega = 0.01$, show no enhancement, due to increasing perturbation, that arises from varying g. Indeed, the maximum response amplitude ($Q_{max} = 1.0$), is obtained when the amplitude of the HF signal, $g = 0$. The response amplitude, Q, monotonously decreases, afterwards, for all values of g. It is worth mentioning, that the VR phenomenon fails to exist in this case, because the maximum response, Q_{max}, is obtained without the amplitude of the HF signal (i.e., $g = 0$).

Understanding the response behaviour of the system, in relation to the LF acoustic excitation, is crucial, particularly, the resonant state, which predefines the enhancement regimes of a dynamical system. In other words, since the ability of a Helmholtz resonator to amplify sound pressure at different frequencies, is a function of its resonant frequency, which depends on the resonator's dimension (ratio of the volume to the neck size), therefore, it is important to understand its operational frequency range. Additionally, the significance of exploring this, cannot be overemphasised. Besides the well-known industrial applications of the HR, for noise control, it has also been recently employed in acoustic energy harvesting [47,49]. The deployment of the HR, to address energy challenges, stems from the fact that the efficiency of a piezoelectric transducer, positioned in the resonator's cavity, is enhanced within the resonant region.

However, while using the theoretical formula directly, to calculate the resonant frequency, is straightforward and efficient, there are cases when the computation error is significant or even incorrect. The deficiencies, arising from the estimated resonant frequency of HRs, in the linear regime only, impose several problems in acoustic theoretical research and engineering applications [48].

Journal: **11071** MS: **10534** TYPESET DISK LE CP Disp.:**2024/11/4** Pages: **21** Layout: **Medium**

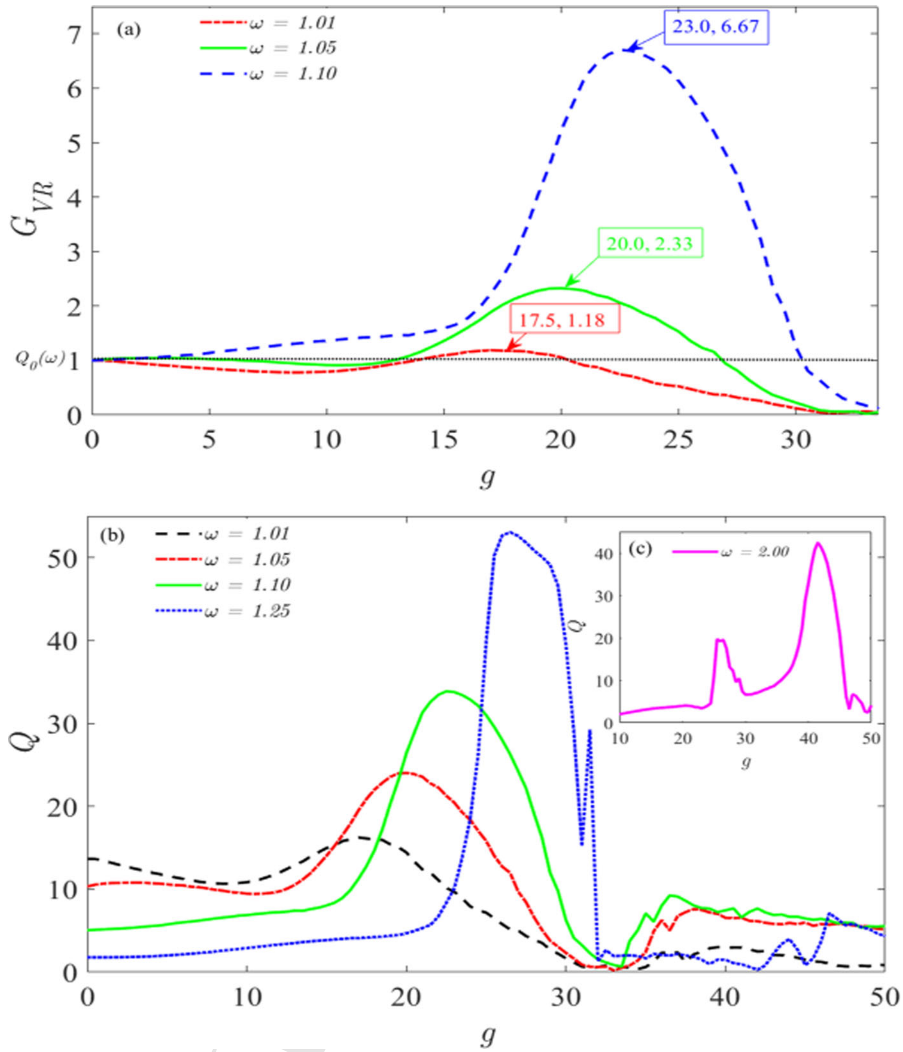

Fig. 12 **a** The gain factor, G_{VR} versus the amplitude of the HF acoustic signal, g, for different values of the LF component, $\omega = [1.01, 1.05, 1.10]$, showing the system's maximum response in the absence of the HF signal (i.e $Q_0(\omega)$). **b** Dependence of response amplitude, Q, on the HF amplitude, g, for different values of the low-frequency component, $\omega = [1.01, 1.05, 1.10, 1.25]$, and **c** $\omega = 2.00$. Other parameters of the system were all fixed at $f = 0.01, \Omega = 6.5, \alpha = 1.2, \beta = 1.36, \sigma = 0.05$, and $\delta = 0.005$

In this study, it is observed that the dynamical behaviour of the air molecules in the HR cavity, respond to both the nonlinearities arising from the resonator's geometry and the acoustic excitation frequency (ω). This, as a result, constitutes the basic features that determine the significant resonant state of the system, as against the size of the HR, alone. Additionally, from the principle of conservation of mass and momentum perspectives, the constituent nonlinearities - the nonlinear restoring force, nonlinear damping, and the external pressure incremental fluctuations, that describe the behaviour of the particles, can define the resonant state of the system, effectively [2,4,45].

Furthermore, in Fig. 14c, the occurrence of double-resonance peaks, when $\omega = 2$, is presented. With the cooperation between the LF component, ω, and the amplitude of the HF signals, g, the magnitude of the observed bi-resonance curve, can be enhanced or suppressed. This is contrary to the insignificant effect of varying f, on the response amplitude of the system, shown in Fig. 14a. Therefore, the possibility of controlling the system's response increases, with an appropriate choice of ω and the HF signal. To complement our discussion on the effect of nonlinearities on the system's response amplitude, the variation of Q, with increasing HF amplitude, g, for different dissipation values, in Fig. 15a and b, is pre-

Journal: 11071 MS: 10534 TYPESET DISK LE CP Disp.:2024/11/4 Pages: 21 Layout: Medium

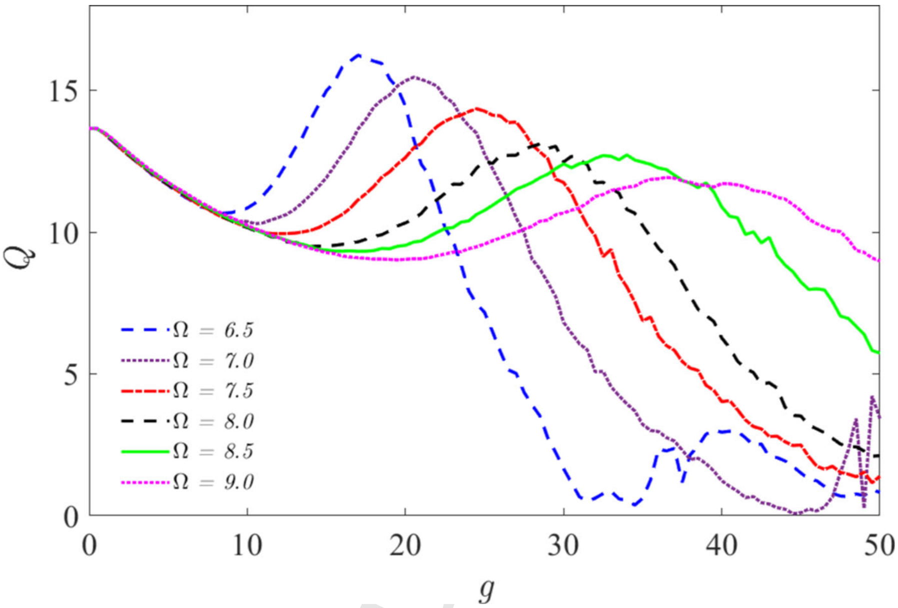

Fig. 13 Dependence of response amplitude, Q, on the HF amplitude, g, for six different values of the HF component, $\Omega = [6.5, 7.0, 7.5, 8.0, 8.5, 9.0]$, with other parameters of the system fixed at $f = 0.01, \omega = 1.01, \alpha = 1.2, \beta = 1.36, \sigma = 0.05$, and $\delta = 0.005$

sented. In Fig. 15a, the dependence of Q on g, for five different values of the linear damping parameter, $\delta = [0.005, 0.010, 0.050, 0.090, 0.120]$ with $\sigma = 0.05$, is shown. Clearly, the maximum response, Q_{max}, of the single VR curve, decreases with increasing δ. Also, varying σ, the nonlinear damping term, produced similar effect. This is shown in Fig. 15b, for $\sigma = [0.03, 0.04, 0.05, 0.06, 0.10]$, and $\delta = 0.005$. Other system parameters were fixed at $\alpha = 1.2, \beta = 1.36, \Omega = 6.5, \omega = 1.01$, and $f = 0.01$.

In Fig. 16, a three-dimensional plot, illustrating the numerically computed response amplitude, Q, as a function of the components of the LF acoustic signal, is presented. The dependence of the response amplitude, on the LF amplitude, f, and LF component, ω, in the range $(f, \omega) \in [(0, 2), (0, 2)]$, with $\alpha = 1.2, \beta = 1.36, \sigma = 0.05$, and $\delta = 0.005$, shows the significant impact of the amplitude of the HF signal, g, on the response dynamics of the system. Aside the decrease in response amplitude, the difference between the resonance regimes is worth noting, as shown in Fig. 16. We remark that the HF amplitude, shifts the regimes of strong resonance towards the low values of f, as shown in Fig. 16b, compared to the curve in Fig. 16a. This implies that the activation of the HF signal, favours the oscillation of the particle in the periodic regimes, thus, corroborating the discussion of our Fig. 6b. The curved surface of the HR's response amplitude, Q, as a function of the components of the HF signal, is shown in Fig. 17. In addition to the effects of the parameters of the low-frequency forcing, in determining the periodic regimes, it also influences the amplitude of the high-frequency acoustic field, g, which is periodic with Ω, hence, optimizes the amplitude, g, that enhances the system's dynamics. The enhancement is significantly pronounced, when the high-frequency parameter is such that $5 \leq \Omega < 15$. The occurrence of resonance, in Fig. 17, is consistent with Fig. 13. The induced resonance, by parameters of the HF signal, in Fig. 17, indicates the possibility of controlling the system's response, by altering g or Ω. In practical terms, this could be achieved through an amplifier. Moreover, the dark red regions on the plot, clearly indicate the well-enhanced regimes. This implies that, with the cooperation of the LF component, ω, and the components of the HF signal (g and Ω), the occurrence of two significant resonance peaks, is possible, particularly when the air molecules are in a periodic motion.

5 Conclusion

In this paper, the oscillations of acoustically-forced air molecules, in a cavity, using the HR model, was examined. Furthermore, the occurrence of VR of the air molecules, describing the resonance behaviour of

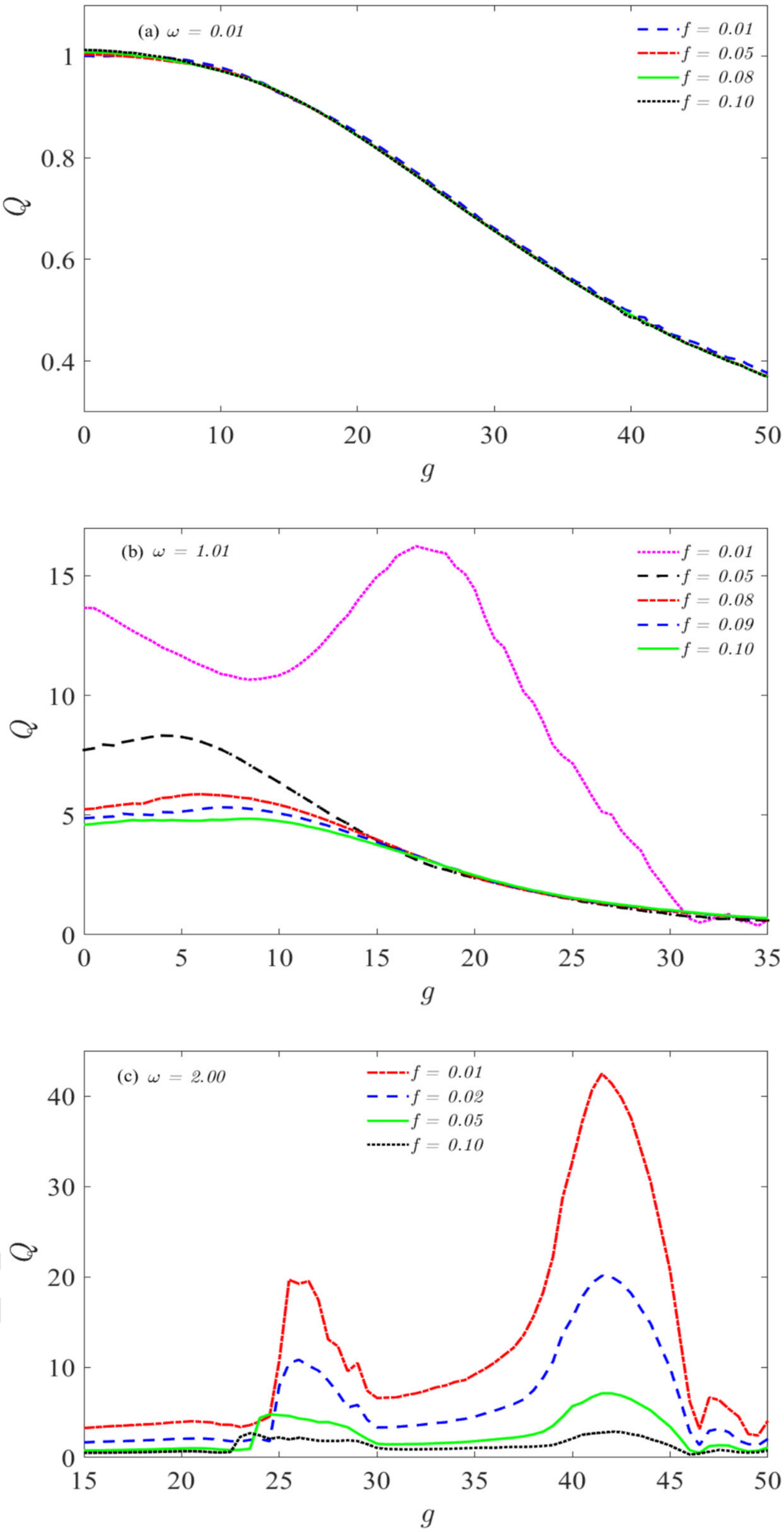

Fig. 14 Variation of the system's response amplitude, Q, with increasing HF amplitude, g, for varying values of the components of the LF signal; **a** $\omega = 0.01$, and $f = [0.01, 0.05, 0.08, 0.10]$; **b** $\omega = 1.01$, with $f = [0.01, 0.05, 0.08, 0.10]$; **c** for $\omega = 2.00$, and $f = [0.01, 0.02, 0.05, 0.10]$. Other parameters of the system were fixed at $\alpha = 1.2, \beta = 1.36, \Omega = 6.5, \sigma = 0.05$, and $\delta = 0.005$

Journal: **11071** MS: **10534** TYPESET DISK LE CP Disp.:**2024/11/4** Pages: **21** Layout: **Medium**

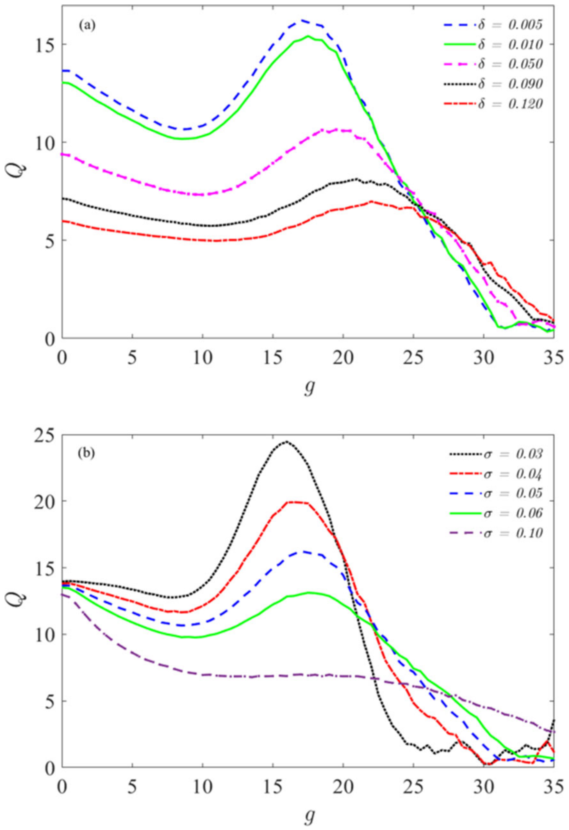

Fig. 15 Dependence of the response amplitude, Q, on the HF amplitude, g, for varying values of both the linear and nonlinear damping parameters; **a** for linear damping, $\delta = [0.005, 0.010, 0.050, 0.090, 0.120]$ with $\sigma = 0.05$, and **b** for nonlinear damping, $\sigma = [0.03, 0.04, 0.05, 0.06, 0.10]$; when $\delta = 0.005$. Other parameters of the system were fixed at $\alpha = 1.2$, $\beta = 1.36$, $\Omega = 6.5$, $\omega = 1.01$, and $f = 0.01$

the HR, was reported. The influence of dual-frequency acoustic forcing, on the system's response, was numerically analysed, and it was demonstrated that all the components of the incident sound pressure, play vital roles in the induction and control of VR. In addition to the appearance of single resonance peak, of the traditional frequency response curve, the realisation of dual-resonance curves, was shown with the appropriate settings of the acoustic field frequencies.

Complementing the previous investigations, of the influence of sound pressure level (SPL), where simultaneous softening and hardening behaviours of the HR was reported [17], it has been demonstrated that the system exhibits other hidden complex dynamics. In particular, it should be noted that the resonator's dynamics, is controlled by its geometry, specific heat ratio, and the acoustic excitation, which determines the nonlinearity and general behaviour of the system. From the application point of view, it is concluded that the roles played by the excitation frequency, is both inductive and contributory. Remarkably, the reported nonlinear behaviours are novel, especially, the system's dynamics at both low and high excitation frequencies. This suggests several design ideas, with advantages that could be explored to maximize the efficiency of acoustic resonators.

Conclusively, the occurrence of VR, with its presence and absence being controlled by the excitation frequency, could facilitate the design of an improved acoustic resonator, an efficient passive sound controller. This finds application in different engineering designs, particularly, in simultaneous noise attenuation and acoustic energy harvesting, where the pressure from acoustic waves vibrates a piezoelectric sensor located in the resonator, to generate electrical energy. Understanding the evolution of air molecules in the resonator and the response dynamics, can increase the amount of energy generated and the efficiency of the acoustic energy harvester. Additionally, the results presented in this paper, provides a logical description of the interaction of the sound waves with the HR. We believe that our new formalism, in describing VR with a HR, and its applications, as enumerated above, paves way to a new body of research and provides a potential application for the development of advanced acoustic metamaterials. Moreover, future work can be focused on investigating the occurrence of VR, analytically, to further elucidate the system's dynamics.

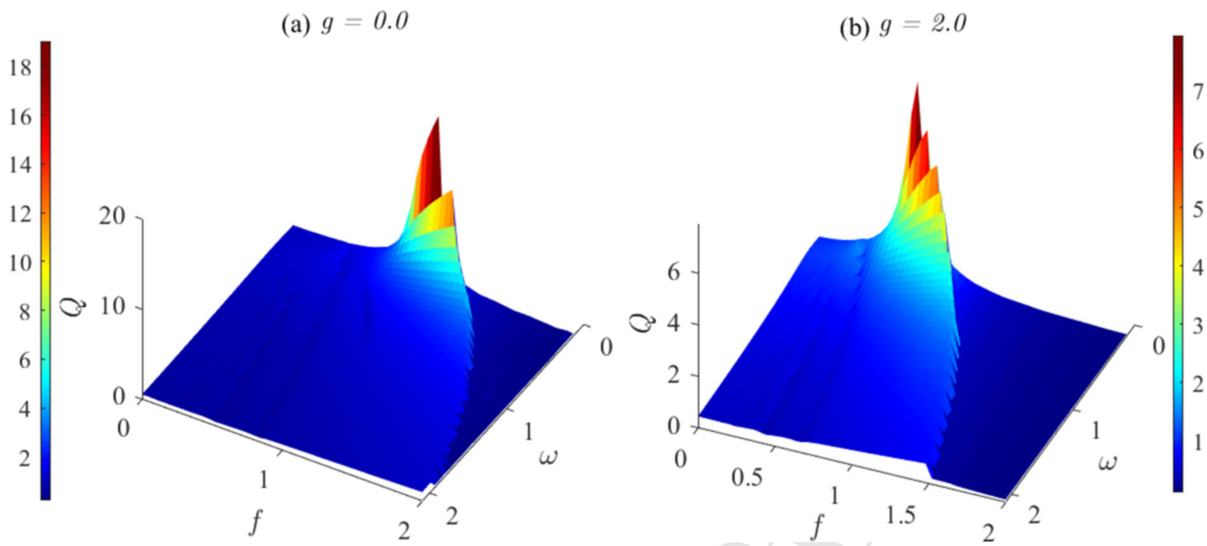

Fig. 16 Three-dimensional plot showing the dependence of the response amplitude, Q, on the LF components (f and ω), for the HF amplitude; **a** $g = 0$ and $\Omega = 0.0$, and **b** $g = 2.0$ and $\Omega = 10$, when other system parameters are set at $\alpha = 1.2$, $\beta = 1.36$, $\sigma = 0.05$, and $\delta = 0.005$

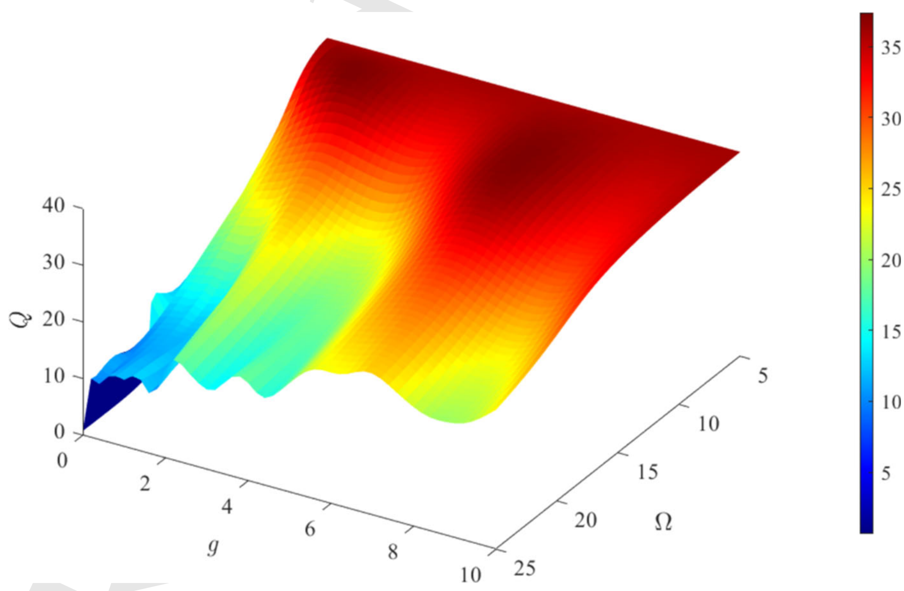

Fig. 17 Three-dimensional plot showing the dependence of the response amplitude, Q, on the HF components (g and Ω), when other system parameters are set at $f = 0.083$, $\omega = 1.01$, $\alpha = 1.2$, $\beta = 1.36$, $\sigma = 0.05$, and $\delta = 0.005$

Funding There is no research funding attached to this research.

References

1. Vincent, U.E., Kolebaje, O.: Introduction to the dynamics of driven nonlinear systems. Contemp. Phys. **61**(3), 169–192 (2020). https://doi.org/10.1080/00107514.2020.1850003

Journal: **11071** MS: **10534** TYPESET DISK LE CP Disp.:**2024/11/4** Pages: **21** Layout: **Medium**

2. Rajasekar, S., Sanjuán, M.A.F.: Nonlinear Resonances, Springer Series in Synergetics. Springer, Switzerland (2016)
3. Vincent, U.E., McClintock, P.V.E., Khovanov, I.A., Rajasekar, S.: Vibrational and stochastic resonances in driven nonlinear systems. Philos. Trans. R. Soc. A **379**(2192), 20200226 (2020). https://doi.org/10.1098/rsta.2020.0226
4. Yang, J., Rajasekar, S., Sanjuán, M.A.F.: Vibrational resonance: a review. Phys. Rep. **1067**, 1–62 (2024). https://doi.org/10.1016/j.physrep.2024.03.001
5. Roy-Layinde, T.O., Omoteso, K.A., Diala, U.H., Runsewe, J.A., Laoye. J.A.: Analysis of vibrational resonance in an oscillator with exponential mass variation. Chaos Solit. Fractals. 178, 114310 (2024). https://doi.org/10.1016/j.chaos.2023.114310
6. Landa, P.S., McClintock, P.V.E.: Vibrational resonance. J. Phys. A Math. Gen. **33**(45), L433 (2000)
7. Blekhman, I.I.: Vibrational Mechanics Nonlinear dynamic effects, general approach, Applications. World Scientific, Singapore (2000)
8. Gammaitoni, L., Hänggi, P., Jung, P., Marchesoni, F.: Stochastic resonance. Rev. Mod. Phys. **70**, 223 (1998)
9. Gandhimathi, V.M., Rajasekar, S., Kurths, J.: Vibrational and stochastic resonances in two coupled overdamped anharmonic oscillators. Phys. Lett. A **360**(2), 279 (2006)
10. Oyeleke, K.S., Olusola, O.I., Vincent, U.E., Ghosh, D., McClintock, P.V.E.: Parametric vibrational resonance in a gyroscope driven by dual-frequency forces. Phys. Lett. A 387, 127040 (2020). https://doi.org/10.1016/j.physleta.2020.127040
11. Fossen, T.I., Nijmeijer, H.: Parametric Resonance in Dynamical Systems. Springer, Berlin (2011)
12. Caldwell, N.B., Daqaq, M.F.: Exploiting the principle parametric resonance of an electric oscillator for vibratory energy harvesting. Appl. Phys. Lett. **110**(9), 093903 (2017). https://doi.org/10.1063/1.4977835
13. Fajans, J., Frièdland, L.: Autoresonant (nonstationary) excitation of pendulums, Plutinos, plasmas, and other nonlinear oscillators. Am. J. Phys. **69**(10), 1096 (2001)
14. Chizhevsky, V.N., Smeu, E., Giacomelli, G.: Experimental evidence of “Vibrational Resonance” in an optical system. Phys. Rev. Lett. **91**, 220602 (2003). https://doi.org/10.1103/PhysRevLett.91.220602
15. Roy-Layinde, T.O., Omoteso, K.A., Oyero, B.A., Laoye, J.A., Vincent, U.E.: Vibrational resonance of ammonia molecule with doubly singular position-dependent mass. Eur. Phys. J. B 95(5), 80 (2022). https://doi.org/10.1140/epjb/s10051-022-00342-9
16. Omoteso, K.A., Roy-Layinde, T.O., Laoye, J.A., Vincent, U.E., McClintock, P.V.E.: Acoustic vibrational resonance in a Rayleigh-Plesset bubble oscillator. Ultrason. Sonochem. 71, 105346 (2020). https://doi.org/10.1016/j.ultsonch.2020.105346
17. Alamo Vargas, V., Gourdon, E., Ture Savadkoohi, A.: Nonlinear softening and hardening behavior in Helmholtz resonators for nonlinear regimes. Nonlinear Dyn. **91**(1), 217 (2018)
18. Lu, Q., Li, X., Zhang, X., Lu, M., Chen, Y.: Perspective: acoustic metamaterials in future engineering. Engineering **17**, 22 (2022)
19. Cummer, S.A., Schurig, D.: One path to acoustic cloaking. New J. Phys. **9**(3), 45 (2007)
20. Popa, B.I., Zigoneanu, L., Cummer, S.A.: Experimental acoustic ground cloak in air. Phys. Rev. Lett. 106(25), 253901 (2011). https://doi.org/10.1103/PhysRevLett.106.253901
21. Ni, X., He, C., Sun, X.-C., Liu, X., Lu, M.-H., Feng, L., Chen, Y.-F.: Topologically protected one-way edge mode in networks of acoustic resonators with circulating air flow. New J. Phys. **17**(5), 053016 (2015)
22. Peano, V., Brendel, C., Schmidt, M., Marquardt, F.: Topological phases of sound and light. Phys. Rev. X 5(3), 031011 (2015). https://doi.org/10.1103/PhysRevX.5.031011
23. Climente, A., Torrent, D., Sánchez-Dehesa, J.: Sound focusing by gradient index sonic lenses. Appl. Phys. Lett. (2010). https://doi.org/10.1063/1.3488349
24. Zhao, J., Bonello, B., Boyko, O.: Focusing of the lowest-order antisymmetric Lamb mode behind a gradient-index acoustic metalens with local resonators. Phys. Rev. B **93**(17), 174306 (2016). https://doi.org/10.1103/PhysRevB.93.174306
25. Ma, G., Yang, M., Xiao, S., Yang, Z., Sheng, P.: Acoustic metasurface with hybrid resonances. Nat. Mater. **13**(9), 873 (2014)
26. Romero-García, V., Theocharis, G., Richoux, O., Merkel, A., Tournat, V., Pagneux, V.: Perfect and broadband acoustic absorption by critically coupled sub-wavelength resonators. Sci. Rep. **6**(1), 19519 (2016). https://doi.org/10.1038/srep19519
27. Sugimoto, N.: Propagation of nonlinear acoustic waves in a tunnel with an array of Helmholtz resonators. J. Fluid Mech. **244**, 55 (1992)
28. Sugimoto, N.: Acoustic solitary waves in a tunnel with an array of Helmholtz resonators. J. Acoust. Soc. Am. **99**(4), 1971 (1996)
29. Bradley, C.E.: Acoustic bloch wave propagation in a periodic waveguide. Tech. rep., Technical Report of Applied Research Laboratories, Report No. ARL-TR-91-19 (July), The University of Texas at Austin (1991)
30. Donahue, C.M., Anzel, P.W.J., Bonanomi, L., Keller, T.A., Daraio, C.: Experimental realization of a nonlinear acoustic lens with a tunable focus. Appl. Phys. Lett. (2014). https://doi.org/10.1063/1.4857635
31. Zhang, S., Yin, L., Fang, N.: Focusing ultrasound with an acoustic metamaterial network. Phys. Rev. Lett. **102**(19), 194301 (2009). https://doi.org/10.1103/PhysRevLett.102.194301
32. Liang, B., Yuan, B., Cheng, J.: Acoustic diode: rectification of acoustic energy flux in one-dimensional systems. Phys. Rev. Lett. (2009). https://doi.org/10.1103/PhysRevLett.103.104301
33. Li X.F., Ni X., Lu M.H, He C., Chen Y.F.: Tunable unidirectional sound propagation through a sonic-crystal-based acoustic diode. Phys. Rev. Lett. **106**(8), 084301 (2011). https://doi.org/10.1103/PhysRevLett.106.084301
34. Robillard, J.F., Muralidharan, K., Bucay, J., Deymier, P. A., Beck, W., Barker, D.: Phononic metamaterials for thermal management: an atomistic computational study. Chin. J. Phys. **49**(1), 448 (2011)

Journal: **11071** MS: **10534** ☐ TYPESET ☐ DISK ☐ LE ☐ CP Disp.:**2024/11/4** Pages: **21** Layout: **Medium**

35. Boechler, N., Theocharis, G., Daraio, C.: Bifurcation-based acoustic switching and rectification. Nat. Mater. **10**(9), 665 (2011)
36. Zhang, J., Romero-García, V., Theocharis, G., Richoux, O., Achilleos, V., Frantzeskakis, D.J.: High-amplitude sound propagation in acoustic transmission-line metamaterial. Appl. Phys. Lett. (2021). https://doi.org/10.1063/5.0040702
37. Lan, J., Li, Y., Yu, H., Li, B., Liu, X.: Nonlinear effects in acoustic metamaterial based on a cylindrical pipe with ordered Helmholtz resonators. Phys. Lett. A **381**(13), 1111 (2017)
38. Gourdon, E., Alexander, N.A., Taylor, C.A., Lamarque, C.H., Pernot, S.: Nonlinear energy pumping under transient forcing with strongly nonlinear coupling: Theoretical and experimental results J. Sound Vib. **300**(35), 522 (2007) https://doi.org/10.1016/j.jsv.2006.06.074
39. Manevitch, L.I., Kovaleva, A.S., Manevitch, E.L.: Limiting phase trajectories and resonance energy transfer in a system of two coupled oscillators. Math. Probl. Eng. (2010). https://doi.org/10.1155/2010/760479
40. Singh, D.K., Rienstra, S.W.: in *19th AIAA/CEAS Aeroacoustics Conference* (2013), p. 2223
41. Förner, K., Temiz, M.A., Polifke, W., Arteaga, I.L., Hirschberg, A.: in *Proceedings of the 22nd International Conference on Sound and Vibration* (2015), 2015–1341
42. Vakakis, A.F.: Inducing Passive Nonlinear Energy Sinks in Vibrating Systems. J. Vib. Acoust. **123**(3), 324 (2001)
43. Meissner M.: The response of a Helmholtz resonator to external excitation. Part II: Flow-induced resonance. Arch. Acoust. **30**(1), 57 (2004)
44. Dykman, M.I., Luchinsky, D.G., Mannella, R., McClintock, P.V.E., Stein, N.D., Stocks, N.G.: Stochastic resonance in perspective. Il Nuovo Cimento D **17**, 661-683 (1995). https://doi.org/10.1007/BF02451825
45. Fidlin, A.: Nonlinear Oscillations in Mechanical Engineering. Springer-Verlag, Berlin, Heidelberg (2006)
46. Strogatz, S.H.: Nonlinear Dynamics and Chaos with applications in Physics, Biology, Chemistry and Engineering (Perseus Book Publishing. L.L.C, Reading, Massacusetts (1994)
47. Noh, S., Lee, H., Choi, B.: A study on the acoustic energy harvesting with Helmholtz resonator and piezoelectric cantilevers. Int. J. Precis. Eng. Manuf. **14**, 1629 (2013)
48. Li, L., Liu, Y., Zhang, F., Sun, Z.: Several explanations on the theoretical formula of Helmholtz resonator. Adv. Eng. Softw. **114**, 361 (2017). https://doi.org/10.1016/j.advengsoft.2017.08.004
49. Aabid, A., Raheman, M.A., Ibrahim, Y.E., Anjum, A., Hrairi, M., Parveez, B., Parveen, N., Mohammed Zayan, J.: A systematic review of piezoelectric materials and energy harvesters for industrial applications. Sensors **21**(12), 4145 (2021)

Journal: **11071** MS: **10534** TYPESET DISK LE CP Disp.:**2024/11/4** Pages: **21** Layout: **Medium**